Detection of Soot Incandescence and PAHs Fluorescence at the Proximity of the Inverse Diffusion Flame by Using Laser Diagnostics

Noriaki Nakatsuka[1], Yasushi Imoto[1], Jun Hayashi[1],
Miki Taniguchi[2], Kenichi Sasauchi[2], Fumiteru Akamatsu[1]
[1]Osaka University, Suita, Osaka, Japan
[2]Chugai Ro Co., Ltd., Sakai, Osaka, Japan

1 Introduction

In terms of sustainable energy utilization, woody biomass is gathering increased attention as an alternative energy source. One of the serious problems for electric power generation by woody biomass gasification, that is an energy conversion process of the woody biomass, is tar formation. Tar means a compound of many kinds of aromatic hydrocarbons and is also a substance which is variously problematic, clogging pipes when it is cooled to improve volumetric efficiency and condensing before being supplied to the gas engine for electric power generation. One way to reduce tar is by oxidative and thermal cracking by partial combustion of the producer gas in the gas reformer [1], an apparatus stage subsequent to the biomass gasifier. During the partial combustion process of the producer gas, an inverse diffusion flame is formed when oxidizer is supplied to producer gas. Cracking and polymerization of tar occur simultaneously at the proximity of the inverse diffusion flame. This polymerization of tar into soot is, however, a significant problem in the gas reformer. With the inverse diffusion flame, oxidative cracking of formed soot is not possible in the downstream, since the downstream atmosphere is comprised of high-temperature fuel. It is, therefore, important to clarify the mechanisms of soot formation at the proximity of the inverse diffusion flame, and to apply the findings to the reforming of containing tar by means of partial combustion of the producer gas.

Here, polymerized tar grows into soot passing through polycyclic aromatic hydrocarbons (PAHs). For the past several decades, some growth mechanisms of PAHs have been proposed; e.g. “H-abstraction-C_2H_2-addition (HACA)” mechanism by Frenklach [2], “reactive coagulation” mechanism by Hepp et al. [3], “the oxidation of phenyl and naphthyl radicals by O_2” by Marinov et al. [4], “phenyl addition/cyclization (PAC)” mechanism by Shukla et al. [5]. These mechanisms are common to the primary PAH growth followed by abstraction of a hydrogen-atom from the reacting hydrocarbon by a gaseous hydrogen atom shown in Eq. (1) below,

$$\mathrm{A}_i + \mathrm{H} \leftrightarrow \mathrm{A}_{i-} + \mathrm{H}_2 \qquad (1)$$

where, A_i represents an aromatic molecule with i peri-condensed rings, and A_{i-} represents its radical. We can, therefore, point to the possibility of suppression of the soot formation by controlling the hydrogen concentration at the proximity of the combustion region.

Correspondence to: nakatsuka@combu.mech.eng.osaka-u.ac.jp

Experimental study has been performed to clarify the effect of hydrogen concentration in the combustion region on soot formation and the growth of PAHs that is a precursor of soot. In the present study, laser induced incandescence (LII) and laser induced fluorescence (LIF) are used in order to measure soot volume fraction and PAHs concentration, respectively.

2 Experimental Methods and Conditions

Figure 1 shows the schematics of the experimental apparatus. The experimental apparatus consists of the supplying system and the combustion furnace. The supplying system provides the model producer gas, composed of hydrogen, methane, carbon monoxide, carbon dioxide, steam (water vapor) and toluene vapor, at the temperature of producer gas just after the gasification of woody biomass. Volumetric flow rate of each gas compound (with the exception of steam and toluene) is controlled by the mass flow control valve. Steam is supplied as liquid water by the pump and is then vaporized by the primary heater, making moisture content of the model producer gas equalize to that from woody biomass. Toluene, model tar, is supplied to the model producer gas by syringe with a micro feeder. The model producer gas temperature at TC2 is controlled at 500 °C by a secondary heater. An inverse diffusion flame is formed in the combustion furnace as shown in Fig. 1. Gas passage of the combustion furnace is a cross section of 80 mm square.

Table 1 shows the volumetric flow rate of each component of model producer gas based on producer gas derived from Japanese cedar gasified by a rotary kiln gasifier at 600 °C. L_{op} in Table 1 represents liter at 25 °C, 1 bar based on the thermodynamic properties of gases. Cross-sectional mean flow rate of the model producer gas is approximately 0.19 m/s. As shown in Table 1, experimental parameter is an additive amount of hydrogen and inert nitrogen (comparative condition) to the oxidizer. Toluene (C_7H_8) is supplied as a model tar compound. Tar consists of many kinds of hydrocarbons, and persistent compounds in tar are aromatic hydrocarbons derived from lignin in woody biomass [6]. Since the aromatic hydrocarbons derived from lignin are polymerized passing through benzene, toluene and xylenes to form PAHs [7], toluene is one of the most appropriate model compounds of tar for investigating the cracking and polymerization mechanism of the persistent tar [8-10].

Oxidizer is supplied from the bottom part of the experimental furnace and introduced into the ignition point by a stainless slit nozzle penetrating the combustion furnace along the centerline. As shown in Fig. 1, the outer diameter of the stainless nozzle is 8.0 mm and the slit width is 2.5 mm. There are two pillars at 120 degrees that hold up the cap of the nozzle. The inverse diffusion flame shaped in a partial planar shape is formed around the slit portion of the stainless nozzle, as the oxidizer is supplied to the model producer gas. The oxidizer is comprised of 70 % oxygen and 30 % nitrogen (volume fraction). The total flow rate of oxidizer is 3.26 L_{op}/min and the Reynolds number (when slit width is adopted as characteristic length) is approximately 1820. This flame shape is efficient in forming a broad combustion region covering a cross section of the gas passage. The inverse diffusion flame is observed through the double quartz windows forming three sides of the combustion furnace. The burnt model producer gas is sampled at the point indicated as "Gas sample" in Fig. 1 and is analyzed by the integrated gas chromatograph system with direct-hot sampling [11]. After sampling, the burnt gas is dewatered by the drain line and completely burned by the flare stack.

Laser induced incandescence (LII) and laser induced fluorescence (LIF) are utilized at the proximity of the inverse diffusion flames as measurement methods of two-dimensional spatial distributions of soot volume fraction and those of PAHs volume concentration, respectively. Figure 2 shows the schematic illustration of the laser diagnostics of LII and LIF, and Table 2 shows the measurement conditions of LII and LIF, respectively. Two Nd:YAG lasers (Quanta-Ray, Spectra Physics Inc.) are employed as laser sources. The lasers are pulsed at 10 Hz, the laser pulse duration is approximately 8 ns. Laser induced incandescence emission from soot particles is exited at a wavelength of 532 nm (second harmonic) whereas laser induced fluorescence emission from PAHs is exited at a wavelength of 355 nm (third harmonic). Three kinds of cylindrical lenses are used to make a laser beam form a laser sheet that is 200 μm in thickness. The measurement regions of LII and LIF are from the slit of the oxidizer supply nozzle to 20 mm downstream, and from the slit of the oxidizer supply nozzle to 30 mm downstream, respectively. The measurement regions are not flush with the central axis of the oxidizer supply nozzle, but 12 mm in front of the central axis. A high speed digital camera (Phantom Ver. 12.0, Vision Research Inc.) with an image intensifier (C4273MOD, Hamamatsu Photonics Inc.) and a 50-mm focal length, f/1.2 lens (Nikkor, Nikon Inc.) is used for LII signal and LIF signal detection. On the one hand, the detection wavelength of LII signal is restricted in range from 370 nm to 430 nm in order to eliminate C_2 Swan band emission [12] via a band pass optical filter (BPF400-60, Asahi Spectra Co., Ltd.). The 60-ns image intensifier is opened 100 ns after the laser pulse to attenuate PAHs LIF, which has a lifetime of approximately 10 ns to 100 ns [13]. On the other hand, the detection wavelength of LIF signal is restricted in range from 487 nm to 509 nm in order to eliminate laser induced formaldehyde fluorescence [14] via another band pass optical filter (DIF-BP-3, Optical Coatings Japan Co., Ltd.). The 60-ns image intensifier is opened 10 ns after the laser pulse. Whereas laser fluence for LII is set to 220 mJ/cm^2 – in which value the soot volume fraction is approximately proportional to the LII signal intensity – laser fluence for LIF is set to 40 mJ/cm^2 the minimum value for a requisite LIF signal able to eliminate the LII signal from the LIF signal.

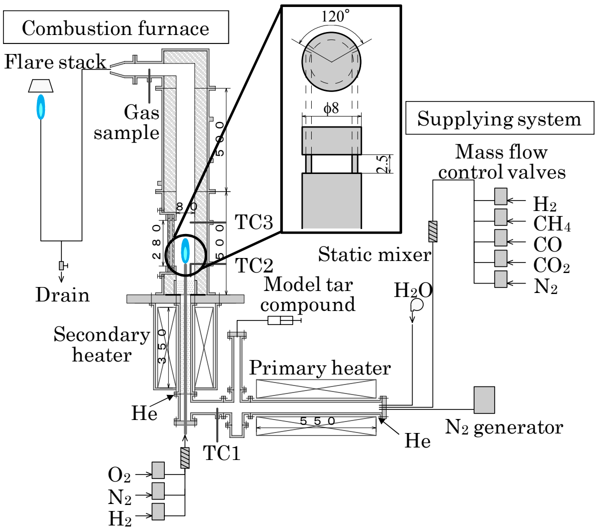

Figure 1. Schematic illustration of the experimental apparatus.

Table 1. Volumetric flow rate of each component of model producer gas in L$_{op}$/min, based on producer gas derived from cedar wood gasified by a rotary kiln gasifier at 600 °C. L$_{op}$: liter at 25°C, 1 bar

		Ⅰ	Ⅱ	Ⅲ	Ⅳ
Model producer gas	H_2	1.60			
	CH_4	2.40			
	CO	4.00			
	CO_2	2.00			
	C_7H_8	0.46			
	H_2O	9.63			
Oxidizer	O_2	2.28			
	N_2	0.98			
	H_2 or N_2	0	0.10	0.20	0.30

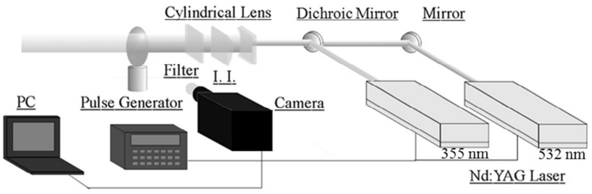

Figure 2. Schematic illustration of the laser diagnostics.

Table 2. Measurement conditions of LII and LIF.

	Soot-LII	PAHs-LIF
Excitation wavelength	532 nm	355 nm
Detection wavelength	370nm~430nm	487nm~509nm
Delay timing	100 ns	10 ns
Gate width	60 ns	60 ns
Laser fluence	220 mJ/cm^2	40 mJ/cm^2

3 Results and Discussion

Figure 3 shows the direct photographs of the inverse diffusion flames. Figure 3 (a) and Fig. 3 (b) show direct observations of hydrogen addition (case 1) and those of nitrogen addition (case 2), respectively. These photographs were taken from the obliquely upper position of the combustion furnace. As shown in Fig. 3, while the luminous intensity of the inverse diffusion flame in case 1 are decreased by the hydrogen addition, those in case 2 are approximately constant with the nitrogen addition.

Figure 4 shows the two-dimensional spatial distributions of the LII signal intensity. White squares in Fig. 3 represent the slit's position. Since the LII signal detections are conducted at 10 Hz which is the same as that of the repetition frequency of the laser, the summations of 1500-time LII signals conducted in the experiment are equivalent to the ensemble-averaged values of 150 s. Contrasting density of white color represents the LII signal intensity which is approximately proportional to the soot volume fraction [12]. Figure 4 (a) and Fig. 4 (b) show two-dimensional spatial distributions of relative soot volume fraction in case 1 and those in case 2, respectively. The summation values of all LII signal intensity in the measurement region are shown in Fig. 5. All summation values are normalized by the value of 0 L_{op}/min condition. As shown in Fig. 4 and Fig. 5, while the LII signal intensity in case 1 are decreased by the hydrogen addition, those in case 2 are approximately constant with the nitrogen addition. In addition, the increase in the amount of hydrogen addition from 0.1 L_{op}/min to 0.3 L_{op}/min hardly affected the LII signal intensity. It can be said that soot formation is suppressed by the chemical effect of a small amount of additional hydrogen (approximately 0.5 % against the total enthalpy of the model producer gas), rather than by a slight change in oxygen concentration and flow velocity of the oxidizer.

Figure 6 shows the two dimensional spatial distributions of the LIF signal. Since the LIF signal detections are conducted at 10 Hz the same as the repetition frequency of the laser, the summations of 1500-time LIF signals conducted in the experiment are equivalent to the ensemble-averaged values of 150 s. Contrasting density of white color represents intensity of the LIF signal from PAHs ranging from 3 to 6-fused aromatic rings [15]. The summation values of all LIF signal intensity are shown in Fig. 7. Contrary to the LII signal, the LIF signal from PAHs is not proportional to the PAHs volume concentration. Several factors must be identical for the relative fluorescence intensity to accurately link PAHs concentrations, including the type of group of molecules being excited, temperature, and the collisional quenching environment. Firstly, the type of group of the PAHs molecules being excited in each additive amount condition can be considered not to be so different since the composition of fuel itself is not changed and detection wavelength (487 nm ~ 509 nm) is relatively narrow. Secondly, the temperature close to the flame (14 mm from the central axis of the nozzle) measured by B-type thermocouple in each of additive amount condition is approximately the same, excluding in 0.3 L_{op}/min hydrogen addition condition as shown in Fig. 8. Finally, the quenching rate for electrically excited PAH molecules is sensitive to the local oxygen concentration, while on the other hand nitrogen, carbon dioxide and water vapor are not expected to quench excited PAHs at appreciable rates [16]. Since oxygen concentration in the region of the intense LIF signal is extremely low, change in lifetime of the PAHs fluorescence is considered to be negligible. Based on the above, the LIF signal intensity of the PAHs are considered to be qualitatively correlated with the volume concentration of the PAHs, excluding the 0.3 L_{op}/min hydrogen addition condition as in this experiment. As shown in Fig. 6 and Fig. 7, the increasing amounts of LIF signal intensity in case 1 is greater than those in case 2. This suggests that the volume concentration of PAHs is increased by the chemical effect of a small amount of additional hydrogen, rather than by a slight change in oxygen concentration and flow velocity of the oxidizer.

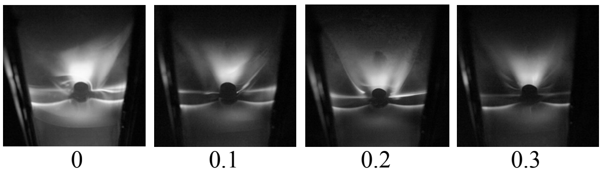

(a) Case 1 (Hydrogen addition) (L_{op}/min)

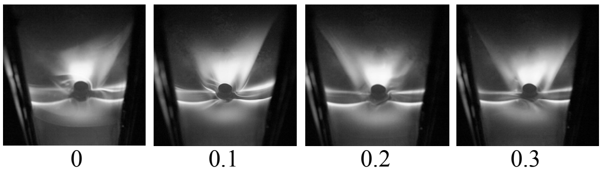

(b) Case 2 (Nitrogen addition) (L_{op}/min)

Figure 3. Direct photographs of the inverse diffusion flames.

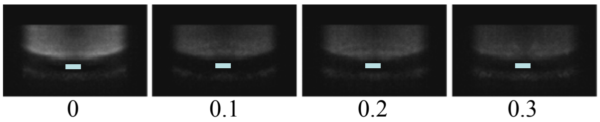

(a) Case 1 (Hydrogen addition) (L_{op}/min)

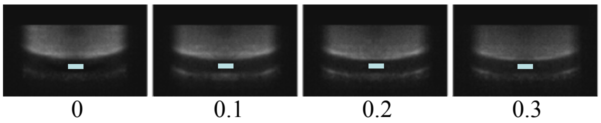

(b) Case 2 (Nitrogen addition) (L_{op}/min)

Figure 4. Two-dimensional spatial distributions of the LII signal whose intensity is approximately proportional to the soot volume fraction [12].

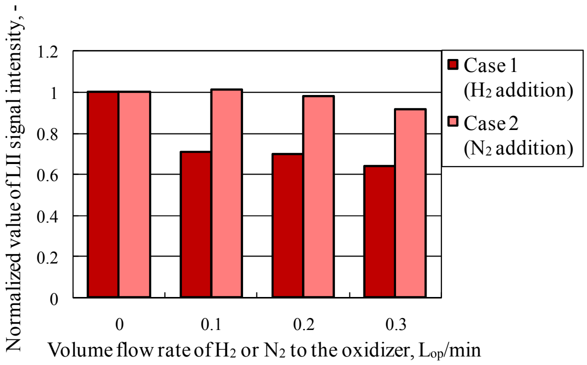

Figure 5. Summation value of all LII signal intensity in the measurement region.

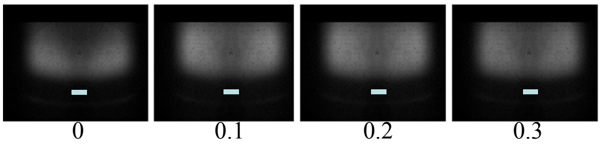

(a) Case 1 (Hydrogen addition) (L$_{op}$/min)

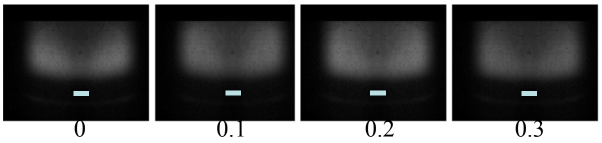

(b) Case 2 (Nitrogen addition) (L$_{op}$/min)

Figure 6. Two-dimensional spatial distributions of the LIF signal whose intensity is qualitatively correlated with the volume concentration of the 3 ~ 6 rings-PAHs.

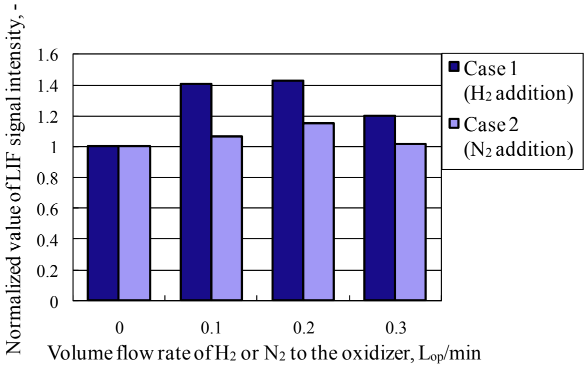

Figure 7. Summation value of all LIF signal intensity in the measurement region.

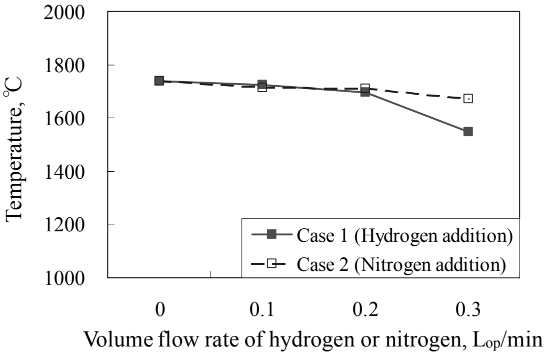

Figure 8. Temperature close to the flame (14 mm from the central axis of the nozzle) measured by B-type thermocouple.

Above mentioned results indicate that the volume fraction of soot decreases whereas the concentration of PAHs (i.e. soot precursors) increases by hydrogen addition to the oxidizer of the inverse diffusion flames. This is because a higher concentration of molecule hydrogen in the combustion region causes a decrease in the forward reaction rate of the hydrogen abstraction reaction of PAHs (Eq. 1), increasing PAHs without active sites. This leads to the lower soot inception from PAHs with active sites formed by the hydrogen abstraction reaction. In addition, the lower soot volume fraction decreases the rate of the surface growth of soot with PAHs, which increases PAHs.

4 Conclusion

As an approach to the problem of soot formation as a consequence of partial combustion of producer gas containing tar, experimental study was conducted to clarify the effect of hydrogen concentration at the proximity of the inverse diffusion flame on soot formation, and the growth of PAHs that is a precursor of soot. In the present study, laser induced incandescence (LII) and laser induced fluorescence (LIF) were used to measure soot volume fraction and PAHs concentration, respectively.

Whereas the LII signal intensity was decreased by hydrogen addition, the signal intensity was maintained relatively constant with nitrogen addition to the oxidizer. Thus, soot formation was suppressed by the chemical effect of a small amount of additional hydrogen (approximately 0.5 % against the total enthalpy of the model producer gas), rather than by a slight change in oxygen concentration and the flow velocity of the oxidizer. Meanwhile, the volume concentration of PAHs was increased by the chemical effect of a small amount of additional hydrogen to the oxidizer. The above results indicate that soot formation was suppressed, whereas the concentration of PAHs (i.e.

soot precursors) increased by hydrogen addition to the oxidizer of the inverse diffusion flames. This occurred because a higher concentration of molecule hydrogen in the combustion region caused a decrease in the forward reaction rate of the hydrogen abstraction reaction of PAHs, increasing PAHs without active sites. This led to the lower soot inception from PAHs with active sites formed by the hydrogen abstraction reaction. In addition, the lower soot volume fraction decreased the rate of the surface growth of soot with PAHs, which increased PAHs.

References

[1] Houben MP, Lange HC, Steenhoven AA, (2005). Tar Reduction through Partial Combustion of Fuel Gas. Fuel, 84: 817-824.

[2] Frenklach, M. (2002). Reaction Mechanism of Soot Formation in Flames. Physical Chemistry Chemical Physics, 11: 2028-2037.

[3] Hepp H, Siegmann K, Sattler K, (1995). New Aspects of Growth Mechanisms for Polycyclic Aromatic Hydrocarbons in Diffusion Flames. Chemical Physics Letters, 233: 16-22.

[4] Marinov NM et al., (1998). Aromatic and Polycyclic Aromatic Hydrocarbon Formation in a Laminar Premixed *n*-Butane Flame. Combustion and Flame, 114: 192-213.

[5] Shukla B, Susa A, Miyoshi A, Koshi M, (2008). Role of Phenyl Radicals in the Growth of Polycyclic Aromatic Hydrocarbons. Journal of Physical Chemistry A, 112: 2362-2369.

[6] Hosoya T et al., (2008). Pyrolysis Gasification Reactivities of Primary Tar and Char Fractions from Cellulose and Lignin as Studied with a Closed Ample Reactor. J. Ana. Appl. Pyrolysis, 83: 71-77.

[7] Waldner MH, Vogel F, (2005). Renewable Production of Methane From Woody Biomass by Catalytic Hydrothermal Gasification. Industrial & Engineering Chemistry Research, 44: 4543-4551.

[8] Swierczynski D, Courson C, Kiennemann A, (2008). Study of Steam Reforming of Toluene Used as Model Compound of Tar Produced by Biomass Gasification. Chem. Eng. and Proc., 47: 508-513.

[9] Taralas G, Kontominas MG, Kakatsios X, (2003). Modeling the Thermal Destruction of Toluene (C_7H_8) as Tar-Related Species for Fuel Gas Cleanup. Energy & Fuels, 17: 329-337.

[10] Bona S, Guillén P, Alcalde JG, García L, Bilbao R, (2008). Toluene Steam Reforming Using Coprecipitated Ni/Al Catalysts Modified with Lanthanum or Cobalt. Chem. Eng. J., 137: 587-597.

[11] Nakatsuka N, Hayashi J, Imoto Y, Taniguchi M, Sasauchi K, Matsuda M, Akamatsu F, (2010). Reforming of Tar in Producer Gas from Woody Biomass: Application of the Inverse Diffusion Flame in the Partial Combustion, Transactions of the Japan Society of Mech. Engineers. B 76: 1637-1645.

[12] Vander Wal RL et al., (1994). Laser-induced incandescence: Development and characterization towards a measurement of soot-volume fraction, Applied Physics B: Lasers and Optics, 59: 445-452.

[13] Mikofski MA, Williams TC, Shaddix CR, Fernandez-Pello AC, Blevins LG, (2007). Structure of laminar Inverse Diffusion Flames, Combustion and Flame, 146: 63-72.

[14] Aizawa T, Kosaka H, (2005). Laser Spectroscopy of Early Soot Formation Process in a Transient Spray Flame: Imaging and Spectral Measurements of Laser-induced Emission at Two Different Excitation Wavelengthes, Transactions of the Japan Society of Mech. Engineers. B 71: 1708-1714.

[15] Aizawa T et al., (2004). Measurements of Excitation-Emission Matrix of PAHs in a Flame Using a Multi-Wavelength Laser Source. Transactions of the Japan Society Mech. Engineers. B 70: 496-502.

[16] Smyth KC, Shaddix CR, Everest DA, (1997). Aspects of soot dynamics as revealed by measurements of broadband fluorescence and flame luminosity in flickering diffusion flames, Combustion and Flame, 111: 185-207.